RAGPPI: Retrieval-Augmented Generation (RAG) Benchmark for Target Identification in Drug Discovery

Anonymous ACL submission

Abstract

Retrieving the biological impacts of protein-protein interactions (PPIs) is essential for target identification (Target ID) in drug development. Given the vast number of proteins involved, this process remains time-consuming and challenging. Large Language Models (LLMs) and Retrieval-Augmented Generation (RAG) frameworks have supported Target ID; however, no benchmark currently exists for identifying the biological impacts of PPIs. To bridge this gap, we introduce the RAG Benchmark for PPIs (*RAGPPI*), a factual question-answer benchmark of 4,420 question-answer pairs that focus on the potential biological impacts of PPIs. Through interviews with experts, we identified criteria for a benchmark dataset, such as a type of QA and source. We built a gold-standard dataset (500 QA pairs) through expert-driven data annotation. We developed an ensemble auto-evaluation LLM that incorporates expert labeling characteristics, average fact–abstract similarity (F_1), and low-similarity fact counts (F_2), enabling the construction of a silver-standard dataset (3,720 QA pairs). We are committed to maintaining *RAGPPI* as a resource to support the research community in advancing RAG systems for drug discovery QA solutions.

1 Introduction

Drug discovery has the potential to yield new therapies that save lives. A historical example is Penicillin, which revolutionized the treatment of bacterial infections and prevented countless deaths since its development in the early 20th century (Drews, 2000). Despite its impact, the discovery process for new drugs remains lengthy and costly: typically spanning about a decade and costing approximately $2 billion to bring a new drug to market (Wouters et al., 2020; Hinkson et al., 2020). One of the key early steps in this time- and cost-intensive process is identifying target proteins to bind to drugs, a process called *target identification* (Target ID).

Target ID aims to identify protein-protein interactions (PPIs), which are protein pathways from an initial protein (IP) to protein candidates for the target protein (TP) (Rasul et al., 2022). TP should have a biological, functional, or physical effect on IP when a drug binds to TP. These impacts ultimately contribute to therapeutic effects for a given disease. However, given that the number of protein candidates in the human body is several billion (Smith and Kelleher, 2013), *Target ID* is very time-consuming and expensive, requiring researchers to explore PPI candidates within the extensive protein space by scanning related literature.

Recently, Large Language Models (LLMs) (OpenAI, 2023; Touvron et al., 2023; Devlin et al., 2019; AI, 2024) have emerged as powerful generative models and have been applied to this protein-related task, where LLMs infer potential biological impacts of protein-protein interactions (PPIs). For example, Tx-LLM (Chaves et al., 2024) is a generalist large language model fine-tuned to encode knowledge across diverse therapeutic modalities and stages of the drug discovery pipeline. JSL-MedLlama-8B (Labs, 2024) is a fine-tuned model based on Llama-8B to support inference of medical QA tasks with a focus on medical genetics. However, they are prone to hallucinations that introduce unreliable results (Ji et al., 2023; Zhang et al., 2023b).

Retrieval-Augmented Generation (RAG) has emerged as a promising solution to alleviate this issue by combining a constantly updated database with efficient information retrieval for more accurate and contextually relevant responses (Lewis et al., 2020; Li and Huang, 2023; Khandelwal et al., 2019). The performance of RAG in improving the reliability of generative models (Martineau et al., 2023; Zhang et al., 2023a) has extended its application to Target ID, where reliability and explainability matter for domain experts. For instance, GraPPI (Li et al., 2025) is a knowledge graph-based RAG

framework employing a retrieve-divide-solve agent pipeline to support large-scale protein-protein interaction exploration for target identification in drug discovery. Instead of using dense vector retrieval, GeneGPT (Jin et al., 2024) trains LLMs to utilize the Web APIs of the National Center for Biotechnology Information (NCBI) for answering genomics questions, employing an augmented decoding algorithm that can handle the function calls of APIs. However, a key challenge in developing RAG for Target ID, despite its potential, is the absence of benchmark datasets for a reliable evaluation. This gap limits the potential applicability of RAG models in Target ID.

We strive to build a benchmark where researchers evaluate their RAG in generating potential biological, functional, or physical effects of PPIs. We present a qualified benchmark dataset for RAG for Target ID through interviews and expert-driven data annotation with 18 domain experts. To further enhance its practical relevance, we developed an automatic evaluation model that captures expert labeling characteristics, thereby demonstrating the benchmark's applicability in real-world biomedical and AI research. Specifically, *RAGPPI* makes three contributions.

- The first contribution is to derive the criteria for creating the dataset through an interview with experts. Our findings established key guidelines for building a benchmark dataset by defining a question type and criteria for the reference. Using BioGrid [1], the most widely adopted dataset for protein-protein interactions (PPIs), we constructed a benchmark dataset to evaluate the potential biological impacts of PPIs, taking into account both the literature frequency and interaction types of PPIs. This means that the dataset, grounded in expert-defined criteria, holds potential to facilitate real-world research on Target ID.

- The second contribution is the benchmark dataset itself. We constructed *RAGPPI*, a factual QA benchmark consisting of 4,420 question-answer pairs on the biological impacts of PPIs. Specifically, through expert-driven data annotation, we first created a gold-standard dataset of 500 PPIs, each annotated with multiple biological steps of downstream processes that ultimately contribute to therapeutic effects for a given disease. Furthermore, leveraging an automatic evaluation model, we generated a silver-standard dataset of 3,720 PPIs, resulting in a total of 4,420 annotated examples. To the best of our knowledge, *RAGPPI* is the first benchmark specifically designed to evaluate Retrieval-Augmented Generation (RAG) models for Target ID.

- The third contribution is a method to scale the dataset synthetically. We developed an ensemble auto-evaluation LLM consisting of three LLMs, each specialized to capture features of expert labeling on "Correct" and "Incorrect" answers. By using an atomic fact-based method (Min et al., 2023), we identified two key features associated with factual inconsistency: 1) average cosine similarity of atomic facts of answers to references, and 2) the number of lower outliers of atomic facts in cosine similarity to references. The ensemble model determines the final label by aggregating predictions from sub-models through majority voting, achieving an accuracy of 93.71%. This enables researchers to leverage our benchmarking dataset without requiring further expert involvement, thereby facilitating broader applicability across the biomedical and NLP communities.

2 Task Formulation Grounded in Expert Interviews

A RAG *QA* system generates an answer *A* to a given question *Q* by leveraging both retrieved external sources and the model's internal knowledge. Domain-specific RAG systems require careful consideration of both QA types and retrieval references. To evaluate such a system in the context of Target ID — a highly specialized domain — it is essential to identify a type of QA and criteria for the references. In the absence of a benchmark for RAG in Target ID, we interviewed domain experts to inform the design of an expert-informed benchmark.

2.1 Interview

We interviewed five drug discovery researchers, four of whom have obtained Ph.D. degrees in chemical engineering, with two working as postdoctoral researchers at a pharmaceutical research center and two working as researchers at a pharmaceutical

[1] https://thebiogrid.org/

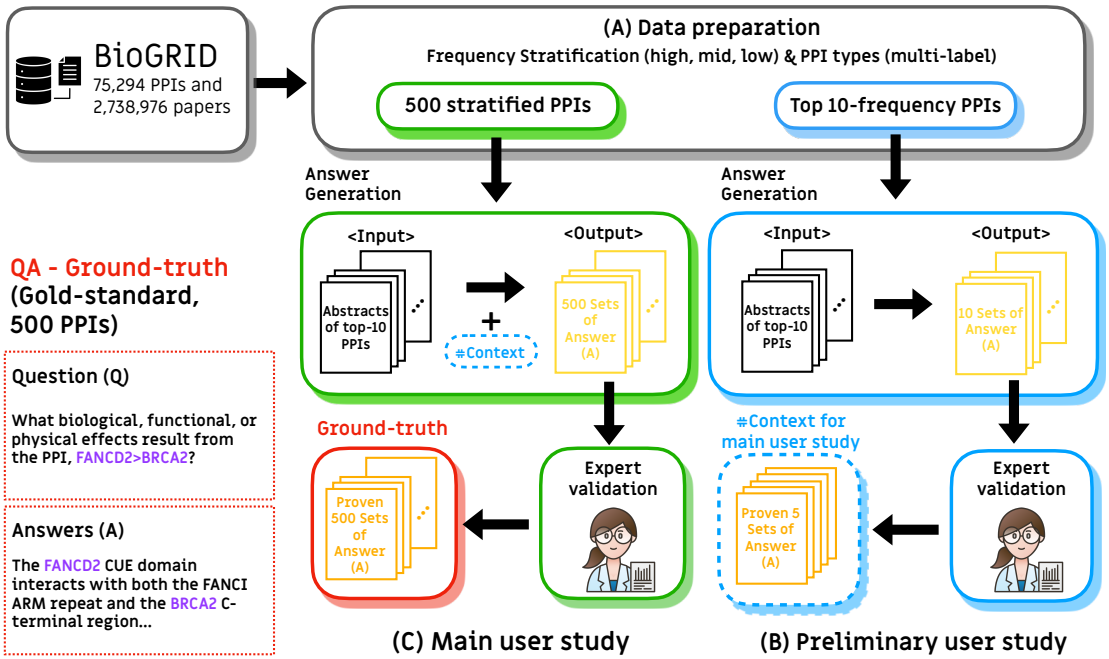

Figure 1: Overview of building the gold-standard dataset. (A) From BioGRID, we extracted the top-10 most frequent PPIs for the preliminary study and 500 stratified PPIs for the main study. (B) Preliminary study: expert validation of the top-10 PPIs provided context for answer generation in the main study. (C) Main user study: expert validation of the 500 stratified PPIs established the ground-truth QA pairs.

company. The fifth researcher is a Ph.D. candidate who has been conducting drug discovery research for the past five years in graduate school. Their work experience ranges from 7 to 10 years (mean=8.75, SD=1.3). Our findings identified 1) a type of information for QA of our benchmark, and 2) which sources to use and how to select them.

Type of QA The key information that experts seek in the context of Target ID is *potential biological impacts of PPIs* that may lead to therapeutic outcomes. Specifically, scientists aim to identify the downstream processes triggered by protein–protein interactions (PPIs) to understand how these interactions contribute to disease. For example, in the Keap1–Nrf2 interaction, chemopreventive agents and oxidative stress inhibit Keap1-mediated degradation of Nrf2. As a result, Nrf2 is stabilized and activates genes with cancer-protective functions, illustrating a therapeutic mechanism against oxidative stress-related diseases.

Criteria for References All experts reported using STRING[2]—a database integrating multiple sources—to search for PPIs. By inputting a specific protein, users can view its associated PPIs along with descriptions based on scientific literature, which are derived from the BioGRID dataset[3].

We identified two criteria for references. First, maintaining a balanced distribution of PPI types is essential, as PPI types are informative for understanding biological processes. This balance implies high generalizability, since it allows coverage of a broader range of PPIs. Table 6 in the appendix lists the seven PPI types: Reaction, Activation, Catalysis, Binding, Ptmod, Inhibition, and Expression. Second, ensuring an even distribution of PPIs across literature frequency levels is important. Frequently studied PPIs support the validation of known mechanisms, whereas infrequently studied ones are often the focus of novel exploration. Thus, literature frequency serves as a strong indicator of potential utility in these workflows.

2.2 Task

Based on the insight from the interviews, we designed an End-to-End RAG task that evaluates how well the output of the RAG model supports the ground-truth biological process. The task is to generate an answer (A) to a question (Q) concerning the biological, functional, or physical effects of protein-protein interactions (PPIs) that contribute

[2]https://string-db.org/

[3]https://thebiogrid.org/

Table 1: Distribution of frequency levels for *RAGPPI*: the gold-standard and silver-standard datasets.

Frequency	Gold-standard (500)	Silver-standard (3,720)	Total (4,220)
High	166 (33.2%)	1,275 (34.3%)	1,441 (34.1%)
Medium	167 (33.4%)	1,246 (33.5%)	1,413 (33.5%)
Low	167 (33.4%)	1,199 (32.2%)	1,366 (32.4%)
Total	500 (100.0%)	3,720 (100.0%)	4,220 (100.0%)

to a therapeutic impact, using evidence derived from BioGRID-curated paper abstracts. These abstracts are selected to ensure a balanced distribution of PPI types and frequencies.

3 Dataset

We constructed a benchmark dataset through three main steps: (1) a gold-standard dataset consisting of 500 expert-verified PPIs collected via a user study; (2) an auto-evaluation model, implemented as an ensemble of LLMs reflecting expert labeling features; and (3) a silver-standard dataset of 3,720 PPIs automatically labeled using an auto-evaluation model. [4]

3.1 Gold-standard dataset

We constructed an expert-verified dataset focusing on a PPI through two main phases: 1) data preparation with BioGRID datasets by PPI type and literature frequency, and 2) expert annotation through user studies.

3.1.1 Data Preparation

In the data preparation phase (Figure 1-A), we conducted frequency stratification and PPI types from the BioGRID dataset (Oughtred et al., 2021) including 2,738,976 PPI samples from 75,294 papers. Stratification prevented the dataset from being overloaded with common diseases (e.g., COVID-19, cancer) and ensured broader coverage, including diabetes, mental disorders, and neurodegenerative diseases.

For frequency stratification, PPIs were categorized into high-, mid-, and low-frequency groups based on their occurrence in the literature. Interactions with a frequency of 1 were labeled as *Low*, while those with frequency ≥ 2 were further divided by computing the mean frequency μ: interactions with frequency $\geq \mu$ were labeled as *High*, and those with frequency $< \mu$ as *Medium*. We extracted 8,066 papers that address only single PPIs to ensure that the benchmark reflects the sufficient retrieval context required for RAG-based QA.

For PPI types, we assigned multi-label annotations to each PPI from seven predefined interaction types—for instance, a kinase might both bind to and phosphorylate its substrate (Binding and Ptmod). After multi-label classification, a dataset with 500 PPIs is created for the following expert's evaluation with equal sampling from each group to mitigate frequency bias while preserving a balanced distribution across the high-, mid, and low-frequency categories (Table 1) and PPI type categories (Table 7 in the appendix). Through these steps, we prepared the top-10 PPIs for the preliminary user study and 500 stratified PPIs for the user study, which are mutually exclusive (Figure 1-A).

3.1.2 Expert Labeling

We conducted preliminary and main user studies in which domain experts validated LLM-generated answers, resulting in a gold-standard dataset of 500 expert-validated PPIs.

Step 1: Preliminary study. Figure 1-B shows the whole process of the preliminary study. We provided GPT-4o with the abstracts of the top-10 PPIs and the template (Table 8 in the appendix) to generate answers, which were evaluated by three experts as perfect, acceptable, or inaccurate.

- Perfect: The response correctly answers the user's question and contains no hallucinated content.
- Acceptable: The response provides a useful answer but may contain minor inaccuracies that do not significantly reduce its utility.
- Incorrect: The response contains incorrect or irrelevant information that fails to address the user's question.

[4] *RAGPPI* will be released under a CC BY 4.0 license and made publicly available upon publication.

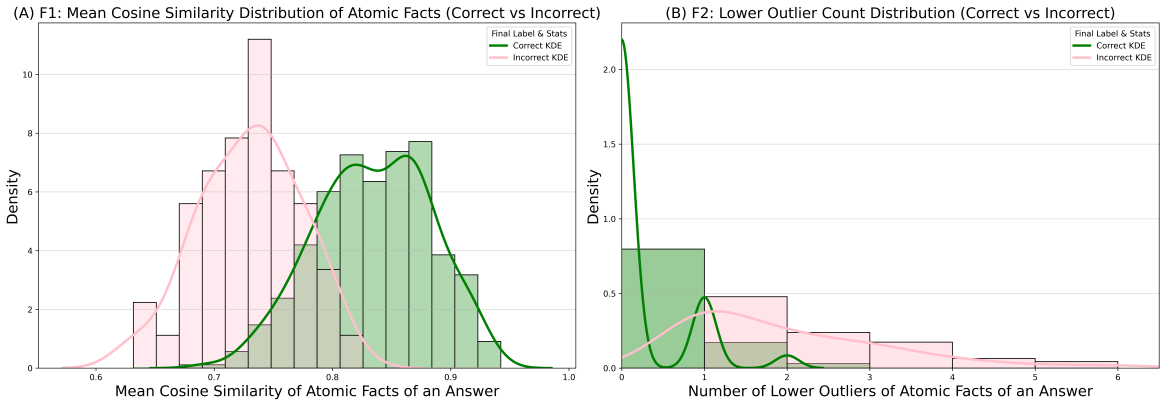

Figure 2: Distributions of semantic features (F_1 and F_2) of Correct (green) and Incorrect (pink) answers based on user study labeling: (A) Distribution of the mean cosine similarity between atomic facts of an answer and its corresponding abstract (F_1); (B) Distribution of the number of atomic facts considered as lower outliers (F_2). Correct answers show higher similarity and fewer outliers compared to Incorrect answers.

Table 2: Distribution of initial and final labels for the 500 PPI dataset. Perfect and Acceptable were merged into the Correct category for final labeling.

Initial label	**# (%)**	**Final label**	**# (%)**
Perfect	383 (76.6%)	Correct	454 (90.8%)
Acceptable	71 (14.2%)		
Incorrect	46 (9.2%)	Incorrect	46 (9.2%)
Total	**500**	**Total**	**500**

We selected 5 PPIs that were rated as perfect by all experts as the final context examples for the LLM in the main user study. Details are provided in § A.2 in the appendix.

Step 2: Main user study. Figure 1-C shows the whole process of the main user study. We provided GPT-4o with the abstracts of the 500 stratified PPIs, the template, and five abstract–answer PPI pairs selected from the preliminary study as context for answer generation. The answers were then evaluated by ten experts as perfect, acceptable, or inaccurate. Based on their review, expert-verified labels were collected, resulting in a ground-truth QA dataset. When answers were labeled as acceptable or inaccurate, the experts were asked to revise them into perfect answers. Details are provided in § A.4 in the appendix.

Step 3: Gold-standard dataset. Table 2 shows the results of expert labeling. The expert-labeled distribution was 383 (76.6%) Perfect, 71 (14.2%) Acceptable, and 46 (9.2%) Inaccurate. We merged the labels, Perfect and Acceptable, into **Correct**, resulting in two final labels, **Correct** and **Incorrect**. We built a gold-standard dataset consisting of 500 QA pairs, each paired with the question and both the corresponding ground-truth and labels.

3.2 Auto-evaluation model

We propose an ensemble-based auto-evaluation model that integrates three sub-LLMs, which are specialized experts' labeling features that distinguish accurate from inaccurate responses: the distribution of average atomic fact-level similarities between each answer and the abstract (F_1), and the distribution of low-similarity atomic facts (F_2). Based on statistical analysis, we identify the expert labeling features and reflect them on each sub-model.

3.2.1 Expert Labeling Features

We characterized the two features (F_1 and F_2) of correct and incorrect answers by measuring how their atomic facts semantically align with the corresponding abstract. F_1 represents the distribution of average atomic fact-level similarities between each answer and the abstract. We decomposed answers and abstracts into atomic facts (Min et al., 2023) by using GPT-4o. For each answer, we compute a cosine similarity of each atomic fact of an answer to each atomic fact of the abstract, and then define the maximum value as the similarity for an atomic fact of an answer. F_1 is the collection of these per-answer averages. F_2 means the distribution of low-similarity atomic facts. For each answer, we count the number of atomic facts whose similarity falls below a threshold (mean minus two standard

Table 3: Results on error rates (ER) for each evaluator. The ensemble model (M1, M2, M3) shows the best performance with the lowest total ER (highlighted in bold), compared to the experts' labeling. Sub-models (M1, M2, M3) are GPT-4 based, each specializing in distinct evaluation perspectives (F_1 and F_2).

Evaluator	**Error Rate(%)**		
	Accurate (35)	**Inaccurate (35)**	**Total (70)**
Expert	0%	0%	0%
Only GPT-4o	31.43%	74.29%	52.86%
GPT-4o with abstract	5.71%	100%	53%
GPT-4o with abstract and GT	0%	83%	42%
M1 (GPT-4o-based)	8.57%	8.57%	8.57%
M2 (GPT-4o-based)	14.29%	2.86%	8.57%
M3 (GPT-4o-based)	2.86%	74.29%	38.57%
Our-Emsenble (M1, M2 and M3)	**2.86%**	**5.71%**	**4.29%**

deviations of F_1, 0.61). F_2 is defined as the collection of these counts. The pseudo algorithm for F_1 and F_2 is shown in Algorithm 1.

An independent t-test was conducted to reveal that Correct exhibits higher cosine similarity and fewer low-similarity outliers compared to Incorrect (Figure 2) In the case of F_1 (Figure 2-A), we observed a significant difference in the cosine similarity of atomic facts of answers to abstract between Correct and Inaccurate ($p < 0.001$). The Correct group had a mean of 0.83 (SD = 0.04), while the Incorrect group had a mean of 0.72 (SD = 0.04). In the case of F_2 (Figure 2-B), we observed a significant difference in the number of low-similarity outliers of atomic facts of answers to abstract between Correct and Inaccurate ($p < 0.001$). The Correct group had a mean of 0.22 (SD = 0.48), while the Incorrect group had a mean of 1.37 (SD = 1.27).

3.2.2 Ensemble LLM for auto-evaluation

We propose an ensemble auto-evaluation model composed of three LLMs (GPT-4o). Two of the sub-LLMs assess factual correctness at the atomic level (F_1 and F_2), while the third evaluates global semantic alignment with the ground truth (GT). We used OpenAI's text-embedding-3-small model[5]. for embeddings to compute the cosine similarity.

- Model-1 (M1): GPT-4o evaluates the answer based on the average cosine similarity between its atomic facts and the corresponding abstract by comparing it with the distribution of GT (Correct: 0.83 $\pm$ 0.04; Incorrect:

Algorithm 1 Computing F_1 (average similarities) and F_2 (low similarity counts)

Input: Answer set $\{A_1, A_2, \ldots, A_n\}$, Abstract set $\{B_1, B_2, \ldots, B_k\}$
Output: Features F_1 and F_2

Input: Answer set $\{A_1, A_2, \ldots, A_n\}$, Abstract set $\{B_1, B_2, \ldots, B_k\}$
Extract atomic facts from Abstract set: $B = \{b_1, b_2, \ldots, b_l\}$
Initialize list S to store per-answer average similarities
Initialize list of lists $\{S_1, S_2, \ldots, S_n\}$ for per-answer fact similarities
for each Answer $A_i \in \{A_1, A_2, \ldots, A_n\}$ **do**
    Extract atomic facts from A_i: $A_i^{\text{facts}} = \{a_1, a_2, \ldots, a_{m_i}\}$
    Initialize list S_i to store representative similarities for A_i
    for each atomic fact $a_j \in A_i^{\text{facts}}$ **do**
        Compute representative similarity: $s_j \leftarrow \max_{k \in \{1,\ldots,l\}} \text{sim}(a_j, b_k)$
        Add s_j to S_i
    end for
    Compute average similarity for A_i: $\bar{S}_i \leftarrow \frac{1}{|S_i|} \sum_{s \in S_i} s$
    Add $\bar{S}_i$ to S
    Store S_i for later use
end for
Set $F_1 \leftarrow S \triangleright F_1$ is the distribution of average similarities
Compute threshold $T \leftarrow \text{mean}(S) - 2 \times \text{std}(S)$
Initialize list L to store low similarity counts per answer
for each S_i in $\{S_1, S_2, \ldots, S_n\}$ **do**
    Compute $L_i \leftarrow$ number of $s_j \in S_i$ where $s_j < T$
    Add L_i to L
end for
Set $F_2 \leftarrow L$ $\triangleright F_2$ is defined as the distribution of low similarity counts per answer
Output: Feature F_1 (distribution), Feature F_2 (low similarity counts)

[5] https://openai.com/index/new-embedding-models-and-api-updates/

0.72 ± 0.04).

- Model-2 (M2): GPT-4o judges the answer by counting the number of atomic facts that are considered lower outliers in their cosine similarity to the abstract and comparing it with the distribution of GT (Correct: 0.22 ± 0.08; Incorrect: 1.37 ± 1.27).

- Model-3 (M3): GPT-4o assesses how well the answer is semantically supported by the ground-truth answer (GT) as a whole.

For each feature, we selected a total of 18 representative examples—three labeled as accurate and three as inaccurate for each model—to serve as demonstrations within the prompt. Each sub-LLM predicts a label as an output. Based on the predictions from the three sub-LLMs, the final label is determined through majority voting.

Table 3 shows the better performance of our ensemble model compared to other models in evaluating responses. To ensure a balanced class distribution in the evaluation, we randomly selected 35 samples from the Correct class and 35 samples from the Incorrect class, excluding those used as examples for the models. In total, 70 samples were used for evaluation. Models prompted with expert-labeled features exhibit more balanced performance across both Correct and Incorrect classes compared to models without such prompts. In contrast, general (non-prompted) models tend to overpredict the Correct label in most cases, highlighting a discrepancy from expert knowledge. Such bias may indicate a potential starting point for hallucination issues in domain-specific tasks. To better understand these discrepancies, we present representative failure cases showing that answers that appear correct to AI models can still be judged incorrect by experts when key therapeutic outcomes are missing (Figure 4 in the appendix).

Algorithm 2 Auto-eval ensemble decision rule for constructing the silver-standard dataset

Input: Labels from Model-1 and Model-2 for answer A
Output: Final decision: "GT" or "Not GT"

```
Input: Model-1 label L1, Model-2 label L2
if L1 = accurate and L2 = accurate then
    return "GT"                ▷ Add to silver-standard dataset
else
    return "Not GT"
end if
```

3.3 Silver-standard dataset

We applied our ensemble auto-eval LLM in generating GT for a silver-standard dataset consisting of 3,720 PPIs. We generated answers for 5,000 randomly selected samples from a total of 8,066 using the same GPT-4o model and prompts employed in constructing the gold-standard dataset (§ 3.1.1). By using M1 and M2 of our ensemble auto-eval LLM, we labeled an AI-generated answer as GT if both M1 and M2 evaluated it as Accurate. Only those answers were included in the final silver-standard dataset. The pseudo algorithm for F_1 and F_2 is shown in Algorithm 2. Consequently, we built *RAGPPI*, a factual question answering benchmark of 4,420 question-answer pairs (Table 1).

4 Benchmarking Experiments

In this section, we present the performance of LLMs and RAG systems on *RAGPPI*, demonstrating that *RAGPPI* has a reasonable level of difficulty and applicability.

Experment setup We tested six systems including two general closed-source LMs: ChatGPT-4.1(gpt-4.1) (OpenAI, 2025) and Gemini-2.0-Flash(gemini-2.0-flash) (Cloud, 2025); one open-source LMs fine-tuned for the biomedical QA task: JSL-MedLlama-3-8B-v2.0 (Labs, 2024); and three biomedical RAG systems: GraPPI (Li et al., 2025), MedRAG (Xiong et al., 2024), and GeneGPT (Jin et al., 2024). We apply the chat template to the open-source model and run inferences with a single A100 GPU. We use Gemini-2.0-flash for the base model in GraPPI and GPT-4.1 for MedGPT. To investigate the quantitative relationship between the quality of retrieval results and overall performance, we compared RAG-based models using their default corpus versus our paper corpus for retrieval. As GeneGPT does not support corpus substitution, it was excluded from the paper-corpus setting. The prompt consists of instructions and five QA pairs as few-shot examples, which are validated by experts (Table 8 in the appendix). We sample 372 PPIs from our database, preserving the distribution of frequency levels and PPI types, and generate biological, functional, or physical effects from each PPI. For each system, a QA pair $\mathscr{P}(Q_{ppi}, A_{sys})$ would be generated. Once the results are generated, the question-answer pairs, $\mathscr{P}(Q_{ppi}, A_{sys1}, A_{sys2}, ..., A_{sys6})$, are passed to our auto-eval LLM.

Table 4: Performance of LLM- and RAG-based models (default and our paper corpus) in terms of atomic fact similarity (F_1), low-similarity fact counts (F_2), and accuracy. The values of F_1 and F_2 are shown as mean and standard deviation. **Bold font** represents the best methods in the evaluation.

Model		Cosine similarity of atomic facts		Accuracy			
		F_1	F_2	M1	M2	M3	Ensemble
LLM-based	GPT-4.1	0.72 ± 0.07	3.09 ± 3.54	52.69%	29.30%	36.83%	39.52%
	Gemini 2.0 flash	0.74 ± 0.13	**0.67 ± 1.53**	58.87%	**67.74%**	11.02%	56.18%
	MedLlama	0.68 ± 0.11	3.39 ± 3.42	39.25%	25.27%	15.86%	25.27%
RAG-based (default corpus)	MedRAG	0.56 ± 0.10	7.53 ± 4.25	8.58%	6.17%	20.38%	8.04%
	GraPPI	0.51 ± 0.20	2.39 ± 3.51	17.20%	17.74%	5.11%	13.44%
	GeneGPT	0.70 ± 0.07	3.68 ± 3.79	45.16%	22.85%	47.31%	35.48%
RAG-based (our corpus)	MedRAG	0.71 ± 0.15	3.36 ± 4.46	55.76%	59.79%	55.50%	55.23%
	GraPPI	**0.76 ± 0.09**	2.46 ± 4.02	**74.26%**	64.61%	**78.28%**	**74.80%**

Results Table 4 shows performance of the LLM- and RAG-based models on the cosine similarity of the atomic facts with the reference (F_1), low-similarity fact counts (F_2), and the accuracy. Overall, RAG models using our paper corpus outperformed both LLM-based models and RAG models with default corpora. GraPPI with our paper corpus achieved the best results, with the highest atomic fact similarity ($F_1 = 0.76$) and ensemble accuracy (74.80%). Given that GraPPI is specialized for protein–protein interaction tasks (Li et al., 2025), this result indicates how domain-specific corpora and domain-specific models complement each other in improving RAG performance.

Interestingly, LLM-based models, despite the absence of retrieval, consistently outperformed RAG models with default corpora. Their higher F_1 and F_2 scores indicate that LLMs generally produce answers aligned with the ground truth, underscoring that an ill-suited corpus can substantially undermine performance. By capturing such contrasts between corpus and model effects, our benchmark effectively evaluates both retrieval and generation, the core processes of RAG. At the same time, LLMs tended to produce generally correct but incomplete answers. For example, Gemini achieves high accuracy in M1 (58.87%) and M2 (67.74%) but low accuracy in M3 (11.02%). While LLMs capture broad factual accuracy, they fail to cover the full scope of domain-specific content. This underscores the importance of ensemble-based approaches that consider both answer-level accuracy (M1 and M2) and alignment with ground-truth that experts validate (M3).

5 Limitation

We present an RAG benchmark for Target ID and an auto-evaluation model, but our study still has some limitations. First, although we built our gold-standard dataset of 500 QA pairs, the number of samples may still be insufficient to cover the full range of biological impacts of PPIs. Second, while we identified the two features with ten experts, their perspectives may not fully capture the expertise of the drug discovery domain. Finally, there is a potential risk that misuse of our benchmark or evaluation model outside expert-supervised research contexts could lead to misleading conclusions in therapeutic discovery. As future work, we plan to collect more annotated data through collaboration with additional experts to enhance the generality of *RAGPPI*.

6 Conclusion

This paper proposes *RAGPPI*, an expert-validated benchmark designed to advance retrieval-augmented generation (RAG) research in target identification. With empirical studies with existing LLMs and RAG models, *RAGPPI* demonstrates its applicability and provides valuable insights for future improvements. We plan to further enhance *RAGPPI* by incorporating insights from additional experts and extending its scope to diverse drug discovery tasks, such as ligand generation and drug repurposing, ensuring that *RAGPPI* remains at the forefront of RAG research and continues to address the evolving needs of the biomedical and NLP research communities.

References

Josh Achiam, Steven Adler, Sandhini Agarwal, Lama Ahmad, Ilge Akkaya, Florencia Leoni Aleman, Diogo Almeida, Janko Altenschmidt, Sam Altman, Shyamal Anadkat, et al. 2023. Gpt-4 technical report. *arXiv preprint arXiv:2303.08774*.

Google AI. 2024. Gemini: Google's large language models. https://gemini.google.com/. Accessed: 2024-08-31.

Juan Manuel Zambrano Chaves, Eric Wang, Tao Tu, Eeshit Dhaval Vaishnav, Byron Lee, S Sara Mahdavi, Christopher Semturs, David Fleet, Vivek Natarajan, and Shekoofeh Azizi. 2024. Tx-llm: A large language model for therapeutics. *arXiv preprint arXiv:2406.06316*.

Google Cloud. 2025. Gemini 2.0 flash | generative ai on vertex ai. Accessed: 2025-05-11.

DeepSeek. 2024. Deepseek-v3. https://deepseek.com/blog/deepseek-v3.html. Accessed: 2025-05-13.

Jacob Devlin, Ming-Wei Chang, Kenton Lee, and Kristina Toutanova. 2019. Bert: Pre-training of deep bidirectional transformers for language understanding. In *Proceedings of the 2019 Conference of the North American Chapter of the Association for Computational Linguistics: Human Language Technologies, Volume 1 (Long and Short Papers)*, pages 4171–4186. Association for Computational Linguistics.

Jurgen Drews. 2000. Drug discovery: a historical perspective. *science*, 287(5460):1960–1964.

Izumi V Hinkson, Benjamin Madej, and Eric A Stahlberg. 2020. Accelerating therapeutics for opportunities in medicine: a paradigm shift in drug discovery. *Frontiers in pharmacology*, 11:770.

Ziwei Ji, Nayeon Lee, Rita Frieske, Tiezheng Yu, Dan Su, Yan Xu, Etsuko Ishii, Ye Jin Bang, Andrea Madotto, and Pascale Fung. 2023. Survey of hallucination in natural language generation. *ACM Computing Surveys*, 55(12):1–38.

Qiao Jin, Yifan Yang, Qingyu Chen, and Zhiyong Lu. 2024. Genegpt: Augmenting large language models with domain tools for improved access to biomedical information. *Bioinformatics*, 40(2):btae075.

Urvashi Khandelwal, Omer Levy, Dan Jurafsky, Luke Zettlemoyer, and Mike Lewis. 2019. Generalization through memorization: Nearest neighbor language models. *arXiv preprint arXiv:1911.00172*.

John Snow Labs. 2024. Jsl-medllama-3-8b-v2.0. Accessed: 2025-05-11.

Patrick Lewis, Ethan Perez, Aleksandra Piktus, Fabio Petroni, Vladimir Karpukhin, Naman Goyal, Heinrich Küttler, Mike Lewis, Wen-tau Yih, Tim Rocktäschel, et al. 2020. Retrieval-augmented generation for knowledge-intensive nlp tasks. *Advances in Neural Information Processing Systems*, 33:9459–9474.

Mingchen Li and Lifu Huang. 2023. Understand the dynamic world: An end-to-end knowledge informed framework for open domain entity state tracking. In *Proceedings of the 46th International ACM SIGIR Conference on Research and Development in Information Retrieval*, pages 842–851.

Ziwen Li, Xiang'Anthony' Chen, and Youngseung Jeon. 2025. Grappi: A retrieve-divide-solve graphrag framework for large-scale protein-protein interaction exploration. *arXiv preprint arXiv:2501.16382*.

Chin-Yew Lin. 2004. Rouge: A package for automatic evaluation of summaries. In *Text summarization branches out*, pages 74–81.

Kim Martineau, AI Explainable, and AI Generative. 2023. What is retrieval-augmented generation? *IBM Research Blog*, 22.

Sewon Min, Kalpesh Krishna, Xinxi Lyu, Mike Lewis, Wen-tau Yih, Pang Wei Koh, Mohit Iyyer, Luke Zettlemoyer, and Hannaneh Hajishirzi. 2023. Factscore: Fine-grained atomic evaluation of factual precision in long form text generation. *arXiv preprint arXiv:2305.14251*.

OpenAI. 2023. Chatgpt: Optimizing language models for dialogue. https://openai.com/chatgpt. Accessed: 2024-08-31.

OpenAI. 2025. Introducing gpt-4.1 in the api. Accessed: 2025-05-11.

Rose Oughtred, Jennifer Rust, Christie Chang, Bobby-Joe Breitkreutz, Chris Stark, Andrew Willems, Lorrie Boucher, Genie Leung, Nadine Kolas, Frederick Zhang, et al. 2021. The biogrid database: A comprehensive biomedical resource of curated protein, genetic, and chemical interactions. *Protein Science*, 30(1):187–200.

Azhar Rasul, Ammara Riaz, Iqra Sarfraz, Samreen Gul Khan, Ghulam Hussain, Rabia Zara, Ayesha Sadiqa, Gul Bushra, Saba Riaz, Muhammad Javid Iqbal, et al. 2022. Target identification approaches in drug discovery. In *Drug Target Selection and Validation*, pages 41–59. Springer.

Lloyd M Smith and Neil L Kelleher. 2013. Proteoform: a single term describing protein complexity. *Nature methods*, 10(3):186–187.

Damian Szklarczyk, Annika L Gable, Katerina C Nastou, David Lyon, Rebecca Kirsch, Sampo Pyysalo, Nadezhda T Doncheva, Marc Legeay, Tao Fang, Peer Bork, et al. 2021. The string database in 2021: customizable protein–protein networks, and functional characterization of user-uploaded gene/measurement sets. *Nucleic acids research*, 49(D1):D605–D612.

Damian Szklarczyk, Rebecca Kirsch, Mikaela Koutrouli, Katerina Nastou, Farrokh Mehryary, Radja Hachilif, Annika L Gable, Tao Fang, Nadezhda T Doncheva, Sampo Pyysalo, et al. 2023. The string database in 2023: protein–protein

association networks and functional enrichment analyses for any sequenced genome of interest. *Nucleic acids research*, 51(D1):D638–D646.

Hugo Touvron et al. 2023. Llama: Open and efficient foundation language models. https://github.com/facebookresearch/llama. Accessed: 2024-08-31.

Olivier J Wouters, Martin McKee, and Jeroen Luyten. 2020. Estimated research and development investment needed to bring a new medicine to market, 2009-2018. *Jama*, 323(9):844–853.

xAI. 2024. Grok-2-1212. https://x.ai/blog/grok-2. Accessed: 2025-05-13.

Guangzhi Xiong, Qiao Jin, Zhiyong Lu, and Aidong Zhang. 2024. Benchmarking retrieval-augmented generation for medicine. In *Findings of the Association for Computational Linguistics ACL 2024*, pages 6233–6251.

Shuo Zhang, Liangming Pan, Junzhou Zhao, and William Yang Wang. 2023a. The knowledge alignment problem: Bridging human and external knowledge for large language models. *arXiv preprint arXiv:2305.13669*.

Tianyi Zhang, Varsha Kishore, Felix Wu, Kilian Q Weinberger, and Yoav Artzi. 2019. Bertscore: Evaluating text generation with bert. *arXiv preprint arXiv:1904.09675*.

Yue Zhang, Yafu Li, Leyang Cui, Deng Cai, Lemao Liu, Tingchen Fu, Xinting Huang, Enbo Zhao, Yu Zhang, Yulong Chen, et al. 2023b. Siren's song in the ai ocean: a survey on hallucination in large language models. *arXiv preprint arXiv:2309.01219*.

A Appendix

A.1 Type of PPIs and the distribution

Through expert interviews, we identified seven types of PPIs considered in their workflows (Table 6). Based on this insight, we extracted 500 PPIs with a balanced distribution across these types (Table 5).

A.2 Preliminary user study

To ensure the quality of answers for the main user study, we conducted a preliminary user study. All participants were researching Target ID. Their career experience ranged from 4 to 9 years (mean=6, SD=2.1). Our study was approved by the Institutional Review Board (IRB), and the consent of the participants was sought before the study. Each participant received a $30 gift certificate.

To ensure the generalizability of the context, we selected the top 10 PPIs with the highest frequency. We used GPT-4o in generating answers for this study based on the performance (§ A.3). We feed a prompt containing the abstract of each of the 10 selected PPIs along with the following the question to GTP-4o, and obtain the corresponding answer:

- Question: What biological, functional, or physical effects result from <*PPI*>?

Experts were asked to label 10 sets of answers as Perfect, Acceptable, or Incorrect. Among these, we identified five sets where all three experts labeled the answers as Perfect. These sets were then used as context examples for the generation model in the main user study.

A.3 Model selection

To determine the best model for identifying protein-protein interactions, we evaluated four large language models: GPT-4o (Achiam et al., 2023), gemini-2.0-flash (Cloud, 2025), grok-2-1212 (xAI, 2024), and deepseek-v3 (DeepSeek, 2024). Each model was tasked with answering three sequential questions that were used in the preliminary user study based on ten abstracts.

To assess model performance, we compared their predictions to the ten abstracts using several metrics: **BERTScore** (Zhang et al., 2019), **ROUGE-1**, and **ROUGE-L** (Lin, 2004). Overall, GPT-4o was judged the most effective model due to its consistently strong performance and clear, concise responses. As summarized in Table 5, gpt-4o led in BERT F1, grok-2-1212 topped ROUGE-L F1 and BERT Precision, and deepseek-v3 ranked highest in ROUGE-1 F1 and BERT Recall.

A.4 Main user study

We recruited 10 professional drug discovery researchers. All participants were researching Target ID. These participants were newly recruited for the *RAGPPI* evaluation, distinct from the formative study. Their career experience ranged from 5 to 18 years (mean=13.5, SD=4.3). Our study was approved by the Institutional Review Board (IRB). Each participant received a $100 gift certificate. Ten experts were asked to label and revise (if necessary) 50 sets of answers as Perfect, Acceptable, or Incorrect. Figure 3 shows the examples of the questionnaires used in this user study.

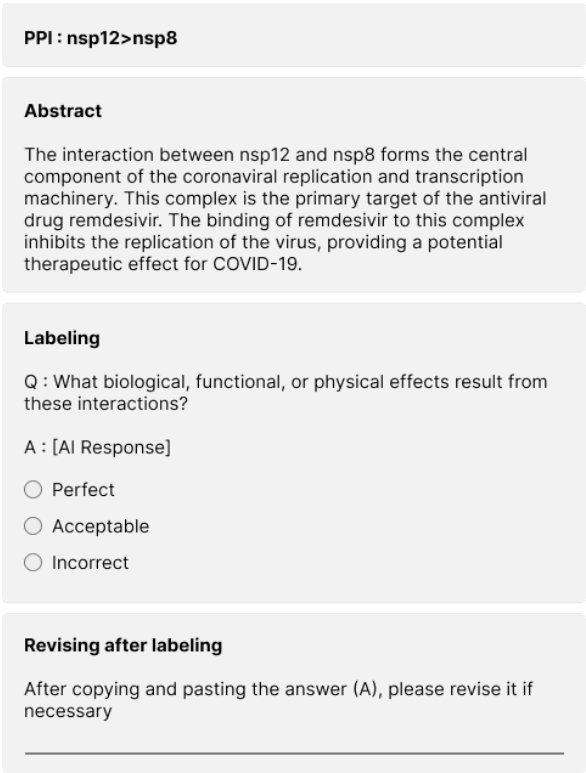

Figure 3: The example of the questionnaire used in our main user study, where experts evaluated an AI-generated answer of the biological or functional effects of PPIs based on the corresponding abstract, and revised them if necessary.

```
PPI: MET>EGFR related to lung cancer

Prediction: Correct
    Model-1: Incorrect | Model-2: Correct | Model-3: Correct | Ensemble: Correct
Ground-truth (GT) by a professional: Incorrect

[Answer]
The interaction between c-MET and EGFR results in the phosphorylation and activation of c-MET,
which in turn positively regulates the activity of EGFR and HER-3, as well as the expression of
their ligands. This leads to c-MET-dependent tumor cell proliferation and migration, and
resistance to apoptosis. However, the c-MET kinase inhibitor INCB28060 can reverse these effects,
suggesting a potential therapeutic strategy for c-MET-driven cancers.

[GT]
And the activated c-MET positively regulates the activity of EGFR and HER-3, as well as the
expression of their ligands.  However, the c-MET kinase inhibitor INCB28060 can reverse these
effects, suggesting a potential therapeutic strategy for c-MET-driven cancers. As a result
INCB28060 potently inhibits c-MET-dependent tumor cell proliferation and migration and effectively
induces apoptosis in vitro.

[Key difference]
The therapeutic effect of this PPI is presented not just at the level of mechanistic inhibition,
but more strongly in terms of concrete cellular outcomes—such as inhibition of proliferation and
migration, and induction of apoptosis—clearly demonstrated in an in vitro context.
```

Figure 4: An example of incorrect prediction by Models.

Model	ROUGE-1 F1	ROUGE-L F1	BERT Precision	BERT Recall	BERT F1
gpt-4o	0.4495	0.2273	0.6625	0.6041	**0.6314**
gemini	0.3284	0.2200	0.6292	0.5369	0.5788
grok-2-1212	0.4468	**0.2342**	**0.6639**	0.5980	0.6289
deepsseek-v3	**0.4673**	0.2189	0.5628	**0.6158**	0.5878

Table 5: Comparison of models on ROUGE and BERT-based evaluation metrics. Bolded values indicate best performance per column.

Table 6: Descriptions and examples of seven PPI types (Szklarczyk et al., 2021, 2023)

PPI Type	Description
Reaction	Proteins participate in the same biochemical reaction or metabolic pathway step, often linked as successive enzymes.
Activation	One protein increases the activity of another, often by direct interaction or signaling.
Catalysis	One protein enzymatically modifies another, such as a kinase phosphorylating a substrate.
Binding	TProteins physically interact to form a complex, either stable or transient.
Ptmod	One protein chemically modifies another after translation.
Inhibition	One protein decreases or suppresses the activity of another protein.
Expression	One protein regulates the expression level (amount produced) of another, typically at the transcriptional level.

Table 7: Distribution of PPI interaction types for *RAGPPI*: the gold-standard and silver-standard datasets.

PPI Types	Gold-standard (500)	Silver-standard (3,720)	Total (4,220)
Reaction	85 (17.0%)	205 (5.5%)	290 (6.9%)
Activation	107 (21.4%)	937 (25.2%)	1044 (24.7%)
Catalysis	86 (17.2%)	231 (6.2%)	317 (7.5%)
Binding	428 (85.6%)	3273 (88.0%)	3701 (87.7%)
Ptmod	122 (24.4%)	1470 (39.5%)	1592 (37.7%)
Inhibition	103 (20.6%)	1108 (29.8%)	1211 (28.7%)
Expression	152 (30.4%)	1470 (39.5%)	1622 (38.4%)
Total	500 (100.0%)	3720 (100.0%)	4220 (100.0%)

Table 8: The prompt template given to systems to generate results for the preliminary study, the main user study, and silver dataset generation. Examples are edited and validated by domain experts in drug discovery. LLM-based systems do not have access to retrieved context.

Question:
"According to the abstract, what biological, functional, or physical effects result from *{$ppi}*? Please answer based on the length and format of the provided example."

Abstract:
{$abstract}

Examples:

Example-1

Abstract:
Missense variants located in the N-terminal region of WDR37 were recently identified to cause a multisystemic syndrome affecting neurological, ocular, gastrointestinal, genitourinary, and cardiac development. WDR37 encodes a WD40 repeat-containing protein of unknown function. We identified three novel WDR37 variants, two likely pathogenic de novo alleles and one inherited variant of uncertain significance, in individuals with phenotypes overlapping those previously reported but clustering in a different region of the protein. The novel alleles are C-terminal to the prior variants and located either within the second WD40 motif (c.659A>G p.(Asp220Gly)) or in a disordered protein region connecting the second and third WD40 motifs (c.778G>A p.(Asp260Asn) and c.770C>A p.(Pro257His)). The three novel mutants showed normal cellular localization but lower expression levels in comparison to wild-type WDR37. To investigate the normal interactions of WDR37, we performed co-immunoprecipitation and yeast two-hybrid assays. This revealed the ability of WDR37 to form homodimers and to strongly bind PACS1 and PACS2 phosphofurin acidic cluster sorting proteins; immunocytochemistry confirmed colocalization of WDR37 with PACS1 and PACS2 in human cells. Next, we analyzed previously reported and novel mutants for their ability to dimerize with wild-type WDR37 and bind PACS proteins. Interaction with wild-type WDR37 was not affected for any variant; however, one novel mutant, p.(Asp220Gly), lost its ability to bind PACS1 and PACS2. In summary, this study presents a novel region of WDR37 involved in human disease, identifies PACS1 and PACS2 as major binding partners of WDR37 and provides insight into the functional effects of various WDR37 variants.

Question 1: According to the abstract, what biological, functional, or physical effects result from the PPI, WDR37>PACS1?

Answer-1: WDR37, a WD40 repeat-containing protein, forms homodimers and binds strongly to PACS1 and PACS2 phosphofurin acidic cluster sorting proteins. However, a novel mutant variant of WDR37, p.(Asp220Gly), loses its ability to bind to PACS1 and PACS2. This loss of interaction could potentially disrupt normal cellular processes, leading to the multisystemic syndrome affecting various aspects of human development, as observed in individuals with this mutation.

Example-2

Abstract:
Menin is a 70-kDa protein encoded by MEN1, the tumor suppressor gene disrupted in multiple endocrine neoplasia type 1. In a yeast two-hybrid system based on reconstitution of Ras signaling, menin was found to interact with the 32-kDa subunit (RPA2) of replication protein A (RPA), a heterotrimeric protein required for DNA replication, recombination, and repair. The menin-RPA2 interaction was confirmed in a conventional yeast two-hybrid system and by direct interaction between purified proteins. Menin-RPA2 binding was inhibited by a number of menin missense mutations found in individuals with multiple endocrine neoplasia type 1, and the interacting regions were mapped to the N-terminal portion of menin and amino acids 43 to 171 of RPA2. This region of RPA2 contains a weak single-stranded DNA-binding domain, but menin had no detectable effect on RPA-DNA binding in vitro. Menin bound

preferentially in vitro to free RPA2 rather than the RPA heterotrimer or a subcomplex consisting of RPA2 bound to the 14-kDa subunit (RPA3). However, the 70-kDa subunit (RPA1) was coprecipitated from HeLa cell extracts along with RPA2 by menin-specific antibodies, suggesting that menin binds to the RPA heterotrimer or a novel RPA1-RPA2-containing complex in vivo. This finding was consistent with the extensive overlap in the nuclear localization patterns of endogenous menin, RPA2, and RPA1 observed by immunofluorescence.

Question 2: According to the abstract, what biological, functional, or physical effects result from the PPI, RPA2>MEN1?

Answer-2: Menin, a tumor suppressor protein, interacts with the RPA2 subunit of the replication protein A (RPA), a protein essential for DNA replication, recombination, and repair. This interaction is disrupted by certain missense mutations in menin found in individuals with multiple endocrine neoplasia type 1. Despite menin's lack of effect on RPA-DNA binding in vitro, it preferentially binds to free RPA2 and may interact with the RPA heterotrimer or a novel RPA1-RPA2-containing complex in vivo, suggesting a potential role in regulating DNA replication and repair processes.

Example-3

Abstract:
FHL1 has been recognized for a long time as a tumor suppressor protein that associates with both the actin cytoskeleton and the transcriptional machinery. We present in this study a paradigm that phosphorylated FHL1 functions as an oncogenic protein by promoting tumor cell proliferation. The cytosolic tyrosine kinase Src interacts with and phosphorylates FHL1 at Y149 and Y272, which switches FHL1 from a tumor suppressor to a cell growth accelerator. Phosphorylated FHL1 translocates into the nucleus, where it binds to the transcription factor BCLAF1 and promotes tumor cell growth. Importantly, the phosphorylation of FHL1 is increased in tissues from lung adenocarcinoma patients despite the down-regulation of total FHL1 expression. Kindlin-2 was found to interact with FHL1 and recruit FHL1 to focal adhesions. Kindlin-2 competes with Src for binding to FHL1 and suppresses Src-mediated FHL1 phosphorylation. Collectively, we demonstrate that FHL1 can either suppress or promote tumor cell growth depending on the status of the sites for phosphorylation by Src.

Question 3: According to the abstract, what biological, functional, or physical effects result from the PPI, FHL1>BCLAF1?

Answer-3: The interaction between FHL1 and BCLAF1, facilitated by the phosphorylation of FHL1 by Src, promotes tumor cell growth. This phosphorylation causes FHL1 to translocate into the nucleus and bind to the transcription factor BCLAF1, switching its role from a tumor suppressor to a cell growth accelerator. However, Kindlin-2 can suppress this process by competing with Src for binding to FHL1, thereby inhibiting FHL1 phosphorylation and its subsequent oncogenic activity.

Example-4

Abstract:
The Kar3 protein (Kar3p), a protein related to kinesin heavy chain, and the Cik1 protein (Cik1p) appear to participate in the same cellular processes in S. cerevisiae. Phenotypic analysis of mutants indicates that both CIK1 and KAR3 participate in spindle formation and karyogamy. In addition, the expression of both genes is induced by pheromone treatment. In vegetatively growing cells, both Cik1::beta-gal and Kar3::beta-gal fusions localize to the spindle pole body (SPB), and after pheromone treatment both fusion proteins localize to the spindle pole body and cytoplasmic microtubules. The dependence of Cik1p and Kar3p localization upon one another was investigated by indirect immunofluorescence of fusion proteins in pheromone-treated cells. The Cik1p::beta-gal fusion does not localize to the SPB or microtubules in a kar3 delta strain, and the Kar3p::beta-gal fusion protein does not localize to microtubule-associated structures in a cik1 delta strain.

Thus, these proteins appear to be interdependent for localization to the SPB and microtubules. Analysis by both the two-hybrid system and co-immunoprecipitation experiments indicates that Cik1p and kar3p interact, suggesting that they are part of the same protein complex. These data indicate that interaction between a putative kinesin heavy chain-related protein and another protein can determine the localization of motor activity and thereby affect the functional specificity of the motor complex.

Question 4: According to the abstract, what biological, functional, or physical effects result from the PPI, CIK1>KAR3?

Answer-4: The interaction between Cik1p and Kar3p, both of which are involved in spindle formation and karyogamy, determines their localization to the spindle pole body (SPB) and microtubules. In the absence of either protein, the other fails to localize to these structures, indicating their interdependence. This interaction likely forms a protein complex that influences the localization of motor activity, thereby affecting the functional specificity of the motor complex.

Example-5

Abstract:
The MYC oncoprotein, also known as the master regulator of genes, is a transcription factor that regulates numerous physiological processes, including cell cycle control, apoptosis, protein synthesis and cell adhesion, among others. MYC is overexpressed in approximately 70% of human cancers. Given its pervasive role in cancer biology, MYC down-regulation has become an attractive cancer treatment strategy.Methods:The CRISPR/Cas9 method was used to produce KO cell models. Western blot was used to analyzed the expressions of MYC and TATA-binding proteinassociated factors 10 (TAF10) in cancer cells (MCF7, A549, HepG2 cells) Cell culture studies were performed to determine the mechanisms by which small molecules (Z363119456, Z363) affects MYC and TAF10 expressions and functions. Mouse studies were carried out to investigate the impact of Z363 regulation on tumor growth.Results:Z363 activate Thyroid hormone Receptor-interacting Protein 12 (TRIP12), which phosphorylates MYC at Thr58, resulting in MYC ubiquitination and degradation and thereby regulating MYC target genes. Importantly, TRIP12 also induces TAF10 degradation, which reduces MYC protein levels. TRIP12, an E3 ligase, controls MYC levels both directly and indirectly by inhibiting MYC or TAF10 activity.Conclusions:In summary,these results demonstrate the anti-cancer properties of Z363, a small molecule that is co-regulated by TAF10 and MYC.

Question 5: According to the abstract, what biological, functional, or physical effects result from the PPI, TRIP12>TAF10?

Answer-5: The activation of TRIP12 by Z363 leads to the phosphorylation of MYC at Thr58, which triggers its ubiquitination and subsequent degradation, thereby regulating MYC target genes. Concurrently, TRIP12 also induces the degradation of TAF10, which further reduces MYC protein levels. This dual action of TRIP12, both directly and indirectly, controls MYC levels and inhibits its activity, demonstrating the potential anti-cancer properties of Z363.